

LETTER TO THE EDITOR

Herschel images of NGC 6720: H₂ formation on dust grains[★]

P.A.M. van Hoof^{1**}, G.C. Van de Steene¹, M.J. Barlow², K.M. Exter³, B. Sibthorpe⁴, T. Ueta⁵, V. Peris¹², M.A.T. Groenewegen¹, J.A.D.L. Blommaert³, M. Cohen⁶, W. De Meester³, G.J. Ferland⁷, W.K. Gear⁸, H.L. Gomez⁸, P.C. Hargrave⁸, E. Huygen³, R.J. Ivison⁴, C. Jean³, S.J. Leeks⁹, T.L. Lim⁹, G. Olofsson¹⁰, E.T. Polehampton^{9,11}, S. Regibo³, P. Royer³, B.M. Swinyard⁹, B. Vandenbussche³, H. Van Winckel³, C. Waelkens³, H.J. Walker⁹, and R. Wesson²

(Affiliations can be found after the references)

Received; accepted

ABSTRACT

Herschel PACS and SPIRE images have been obtained of NGC 6720 (the Ring Nebula). This is an evolved planetary nebula with a central star that is currently on the cooling track, due to which the outer parts of the nebula are recombining. From the PACS and SPIRE images we conclude that there is a striking resemblance between the dust distribution and the H₂ emission, which appears to be observational evidence that H₂ forms on grain surfaces. We have developed a photoionization model of the nebula with the Cloudy code which we used to determine the physical conditions of the dust and investigate possible formation scenarios for the H₂. We conclude that the most plausible scenario is that the H₂ resides in high density knots which were formed after the recombination of the gas started when the central star entered the cooling track. Hydrodynamical instabilities due to the unusually low temperature of the recombining gas are proposed as a mechanism for forming the knots. H₂ formation in the knots is expected to be substantial after the central star underwent a strong drop in luminosity about one to two thousand years ago, and may still be ongoing at this moment, depending on the density of the knots and the properties of the grains in the knots.

Key words. planetary nebulae: individual: NGC 6720 – circumstellar matter – dust, extinction – Infrared: ISM – ISM: molecules

1. Introduction

Grains play an important role in many environments, including planetary nebulae (PNe), because of extinction, photoelectric heating, their influence on the charge and ionization balance of the gas, as catalysts for grain-surface chemical reactions (e.g. H₂ formation), and as seeds for freeze-out of molecules. Previous satellite missions such as IRAS, ISO, Spitzer, and AKARI have allowed us to study the dust in PNe, but unfortunately the angular resolution of these instruments was too low to get detailed information on the spatial distribution of the dust. This has now changed with the launch of Herschel, which allows us to study the spatial structures in unprecedented detail. In this paper we will do this for NGC 6720 (M57, the Ring nebula) to study H₂ formation. NGC 6720 is an evolved, oxygen-rich bipolar nebula seen nearly pole-on. The nebula is optically thick to ionizing radiation in most directions, but optically thin in the polar regions (O'Dell et al. 2007, hereafter OD07). Molecules such as H₂ and CO have been detected (Beckwith et al. 1978; Huggins & Healy 1986). The central star has exhausted hydrogen shell burning and is now on the cooling track. As a result the outer halo is recombining and re-ionization of the innermost recombined material due to expansion of the nebula has just started (OD07). This object is very similar to the Helix nebula, which seems to be further advanced along the same evolutionary path (OD07). In Sect. 2 we will describe the observations, and in Sect. 3 we will discuss various scenarios for the formation of H₂.

2. Observations

The images of NGC 6720 presented in this paper were obtained with the PACS and SPIRE instruments on board the Herschel satellite (Pilbratt et al. 2010) on 2009-10-10 and 2009-10-06, respectively, as part of the Science Demonstration Phase of the Mass-loss of Evolved StarS (MESS) guaranteed time key program (Groenewegen et al., in preparation). The PACS instrument is described by Poglitsch et al. (2010). The SPIRE instrument, its in-orbit performance, and its scientific capabilities are described by Griffin et al. (2010), and the SPIRE astronomical calibration methods and accuracy are outlined by Swinyard et al. (2010). The reduction of our data is described in Appendix A. We also determined the total flux in each of the images. This is described in Appendix B. Below we will discuss these images in detail and compare them to the H₂ morphology of the nebula. To this end we used a ground-based H₂ 2.12 μm image, obtained with the Omega2000 camera on the 3.5-m Zeiss telescope at the Calar Alto Observatory.

In Fig. 1 we present the PACS and SPIRE images and compare them to the Calar Alto H₂ image. The morphology of the dust and the H₂ emission shows a striking resemblance even in small details. This appears to be observational evidence that H₂ forms on grain surfaces in an astrophysical environment. Such evidence is very rare. A similar result was obtained by Habart et al. (2003) for the ρ Ophiuchi molecular cloud, suggesting that H₂ forms on PAH surfaces. The presence of PAHs in NGC 6720 cannot be fully excluded, but seems very unlikely. Accordingly our observations are the first indication for H₂ formation on oxygen-rich dust grains in an astrophysical environment to our knowledge.

[★] Herschel is an ESA space observatory with science instruments provided by European-led Principal Investigator consortia and with important participation from NASA.

^{**} email: p.vanhoof@oma.be

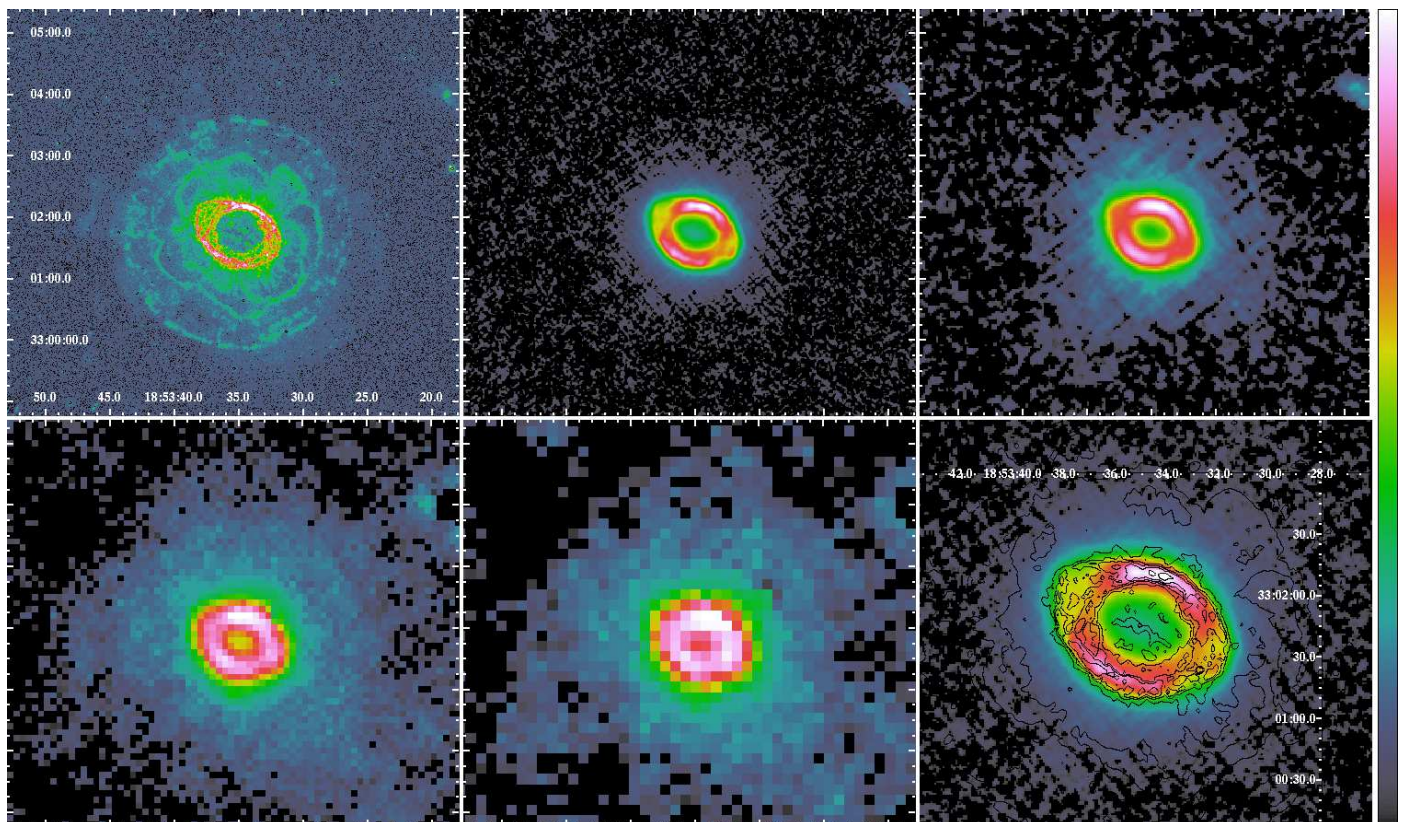


Fig. 1. NGC 6720 in five photometric bands. Top row from left to right: H₂ 2.12 μm , PACS 70 μm , PACS 160 μm . Bottom row from left to right: SPIRE 250 μm , SPIRE 350 μm , and an overlay of the Calar Alto H₂ contours on the PACS 70 μm image. The H₂ image is not flux calibrated. The maps have standard orientation (N to the top, E to the left).

We can divide the H₂ image into 3 regions: the inner ring, with a semimajor axis of $\sim 45''$, an inner set of arcs with a radius of $\sim 70''$ (the inner halo), and an outer set of arcs with a radius of $\sim 110''$ (the outer halo). There is also fainter emission outside of these outer arcs, but this is not very easy to see on the printed map.

Comparing the H₂ and the sub-mm maps it is clear that the size and shape of the inner ring is reproduced on all images. The same can be said for the inner halo, which can be seen clearly on all maps. In the NW part of the inner halo, the H₂ emission region is broader than in the SE—this too is the case on the SPIRE images, and less clearly so on the PACS images. Finally, the outer halo on the H₂ image is also visible on the sub-mm images—as extended emission on the SPIRE images and as a faint circular ring shape on the PACS images (on the 70 μm image most clearly). On the zoomed PACS 70 μm with overlaid H₂ contours (Fig. 1, lower right panel) the clear correspondence between the optical and sub-mm emission in the ring and the inner halo is highlighted.

3. The origin of the H₂

From the ground-based H₂ images it is clear that most of the H₂ resides in high density knots in the inner ring (Speck et al. 2003). In this section we will investigate the origin of this H₂. The halo also shows H₂ emission, which has a very different morphology though. The latter will not be discussed here. It is clear that H₂ was formed in the dense AGB wind. In the post-AGB phase three different scenarios will be investigated: 1) this H₂ survived in the ionized region, 2) this H₂ survived in the knots,

Table 1. Parameters of the Cloudy model of NGC 6720.

T_{eff} (kK)	134.7	$\epsilon(\text{C})$	8.20
L_* (L_{\odot})	239.	$\epsilon(\text{N})$	7.89
r_{in} (mpc)	56.	$\epsilon(\text{O})$	8.50
r_{out} (mpc)	175.	$\epsilon(\text{Ne})$	7.93
$\log(n_{\text{H}})$ (cm^{-3})	2.60	$\epsilon(\text{S})$	6.42
T_e (kK)	11.97	$\epsilon(\text{Cl})$	4.94
$\log(n_e)$ (cm^{-3})	2.62	$\epsilon(\text{Ar})$	6.19
$\log(\Gamma)$	-2.21	$\epsilon(\text{Fe})$	5.18
$\epsilon(\text{He})$	11.00	D (pc)	740.

which formed before the gas was ionized and 3) this H₂ was destroyed and then was formed again later inside the knots when they formed. These scenarios were already investigated for the Helix nebula by Matsuura et al. (2009). In order to determine the physical conditions in the nebula we created a photoionization model using a prerelease of version C10.00 of the photoionization code Cloudy (revision 3862), last described by Ferland et al. (1998). The details of the modeling are described in Appendix C, the resulting model parameters are summarized in Table 1.

3.1. Can H₂ survive in the ionized region?

For the Helix nebula, Matsuura et al. (2009) conclude that “part of the H₂ is primordial, i.e. formed during the AGB phase, and survived the ionization of the nebula”. This conclusion is based on the work of Aleman & Gruenwald (2004, hereafter AG04). We recreated the models of AG04 with Cloudy. This code is capable of creating an equilibrium model of the ionized region as

well as the PDR and the molecular regions. It includes state-of-the-art code for modeling grains (van Hoof et al. 2004) as well as the chemistry network (Abel et al. 2005) and the H₂ molecule (Shaw et al. 2005). We created spherically symmetric, one-dimensional models with the parameters of the standard model of AG04. Our H₂ model includes all ro-vibrational levels of the ground electronic state, as well as the six electronically excited states that are coupled to the ground state by permitted electronic transitions. Self-shielding of the H₂ molecule was calculated self-consistently using detailed radiative transfer (including line overlap) of each of the roughly half a million lines of the molecule.

First we needed to define the outer radius of the ionized region. In PNe that is not straightforward. Due to the ν^{-3} dependence of photoionization cross section, the high energy tail of the stellar spectrum will propagate through the ionized region into the PDR and cause hydrogen to stay partially ionized there. Such PDRs are sometimes referred to as XDRs. The transition from fully ionized gas to neutral gas will be gradual and the transition layer will have a considerable thickness. Aleman & Gruenwald (2004) stopped their calculations when $n(\text{H}^+)/n_{\text{H}} = 10^{-4}$ was reached¹. Cloudy by default stops when the electron temperature drops below 4000 K, based on the notion that at lower temperatures the forbidden optical emission lines will no longer be excited effectively and the stopping radius will coincide with the outer radius in optical images of the nebula. The choice of the stopping criterion is crucial, but is unfortunately not discussed by AG04. The H₂ fraction R_{M} (Eq. 7 in AG04) continually rises as the value of $n(\text{H}^+)/n_{\text{H}}$ where the calculation is stopped, is lower. This is illustrated in Fig. 2. This clearly shows that there is no obvious choice for the stopping criterion: the deeper one integrates, the higher the value of R_{M} becomes. This is hardly surprising: deeper layers are better shielded from UV radiation and the H₂ abundance will be higher. The local maximum of the H₂ abundance that AG04 report around $n(\text{H}^+)/n_{\text{H}} = 0.1$ is barely reproduced in the Cloudy model and has virtually no effect on the overall value of R_{M} (see Fig. 3). Most of the H₂ present in this model will be in regions near the outer radius. The H₂ weighted average ionization of hydrogen is slightly more than 10^{-3} . So a more precise statement would be that a small fraction of H₂ can survive (or better: is constantly destroyed and formed again) in the transition region between the ionized region and the molecular region. The expectation of AG04 that using a detailed treatment of H₂ self-shielding could increase the value of R_{M} by up to 2 dex could not be confirmed with Cloudy, at least not for the standard model of AG04. Our value of R_{M} is actually slightly lower than reported by AG04. The standard model of AG04 is roughly appropriate for a low-mass central star on the horizontal track. To model a high-mass central star, we also created a “standard4” model which is identical to the standard model except that $n_{\text{H}} = 10^4 \text{ cm}^{-3}$ and $L_* = 10^4 L_{\odot}$. The results are shown in Figs. 4 and 5. In this model, the value for R_{M} is somewhat lower than in the standard model. So the conclusion is that a small amount H₂ can exist in the ionized region, mostly in the transition zone towards the PDR, and that this amount is not sufficient to explain the observed H₂ emission in the inner ring.

¹ The number 10^{-4} is stated in the text, but an inspection of their Fig. 1 suggests that they actually used 10^{-3} . In this section we will adopt 10^{-4} as the stopping criterion.

3.2. Can H₂ survive in knots?

When the photoionization of the AGB shell starts at the moment when a planetary nebula is born, the molecules in the circumstellar shell will be very quickly destroyed unless they can somehow be shielded from the ionizing radiation. Dense knots that formed during the AGB phase can provide this environment and seem a very attractive explanation for the existence of H₂ in evolved PNe such as NGC 6720. It is clear that dense knots can shield the material in the center from FUV flux and allow H₂ molecules to survive. But it is also obvious from the images presented in e.g. Matsuura et al. (2009) that the FUV flux will interact with the outer layers of the knot. This interaction causes material to be advected off the knot. During that process the material will be heated, causing H₂ to shine. This provides a natural explanation for the H₂ spectrum seen in the Helix nebula (Henney et al. 2007). This process will gradually erode the knots, and eventually they will be destroyed. We will now make an estimate of the lifetime of a knot in the ionized region.

We adopt a value of $1.5 \times 10^{-5} M_{\odot}$ for the mass of the knots (Meixner et al. 2005; Matsuura et al. 2009). We furthermore assume that the knots have a typical diameter of $0.5''$. Combined with a distance of 740 pc (O’Dell et al. 2009) this gives a physical diameter of $5.54 \times 10^{10} \text{ km}$ (370 AU), in agreement with the typical size stated in O’Dell et al. (2003). Assuming that 70% of the mass is hydrogen, this yields an average number density of hydrogen of $n_{\text{H}} = 1.4 \times 10^5 \text{ cm}^{-3}$. The density in the center of the knot should be higher, in agreement with the measurements by Meaburn et al. (1998) and Huggins et al. (2002). We assume spherical astronomical silicate grains to be present in the knot, with a standard ISM size distribution (Mathis et al. 1977) and a dust-to-gas mass ratio equal to the standard model of NGC 6720.

Henney et al. (2007) state that their models C06 and A06 matched the observations of the Helix nebula best for the outer and inner knots, respectively. Taking the parameters for the advection flow presented in Table 1 of Henney et al. (2007), one can calculate that the erosion rate would be approximately 10^{-10} and $10^{-9} M_{\odot} \text{ yr}^{-1}$ for the C06 and A06 model, respectively. Combining this with the adopted mass of the knot yields a survival time of 15,000 to 150,000 yr. However, one should realize that during most of PN evolution the central star luminosity was much higher than assumed here (by upto 2 dex, the central star of the Helix nebula has a luminosity of $120 L_{\odot}$), and also that the nebula was much more compact during the early stages of evolution causing the knots to be much closer to the central star. This will cause the erosion to be much faster early on and hence the survival time to be much shorter. The erosion rate will scale at least with the square-root of the EUV flux when the advection flow is in the recombination-dominated regime. So a conservative estimate is that the survival time is at least a factor 10 shorter than stated above, and likely more. O’Dell et al. (2007, 2009) state that the kinematic age of the Ring nebula is 7000 yr, making the survival of the knots inside the ionized region problematic. Note that this argument also applies to models where the knots formed due to instabilities at the ionization front during the onset of ionization. More detailed modeling of the knots during the high-luminosity phase is warranted though to reach a more definitive conclusion.

3.3. Can H₂ be formed again after ionization?

O’Dell et al. (2007) argue that knot formation only starts after the central star has entered the cooling track and the nebular material starts recombining. This argument is based on the fact that

no similar features are seen in HST images of younger PNe. We propose a new explanation in which the recombining gas cools very quickly, much faster than the recombination proceeds. This is indicated by Fig. 4 in Ferland & Truran (1981), but these calculations clearly need to be redone for conditions that are more appropriate for NGC 6720. The fast cooling would result in gas that is still ionized (and thus produces abundant recombination radiation) but has very little thermal pressure support. The radiation pressure of the recombination radiation on the dust and/or gas may then cause the medium to become unstable and fragment into many globules.

O'Dell et al. (2007) also argued that the main gas phase of NGC 6720 was fully ionized during the high-luminosity phase, so that any H₂ present in the gas would have been destroyed very quickly (on timescales less than a year). Consequently any H₂ present in the knots must have formed after the formation of the knots itself started and they became dense enough to shield the molecules from the UV light. To investigate this scenario further, we created Cloudy models of the knots using revision 3862 of the experimental “newmole” version of the code in order to cope with the very steep density gradient at the outer edge of the knot. As was the case with the models described in Sect. 3.1, we use a full and self-consistent H₂ model. The models are based on our standard model of NGC 6720, with a modified density law that mimics a dense knot just outside the ionized region. The density is constant until the electron temperature drops below 4000 K, then the density will rise steeply towards the core density of the knot with an assumed scale-length of 2×10^9 km.

We computed eight Cloudy models with $\log n_{\text{H}} = 4(0.5)7.5$ to cover the full range of plausible densities in the center of the knot. From the models we extracted the formation (solid lines) and destruction timescales (dotted lines) of H₂. The results are shown in Fig. 6 for selected models. The Cloudy models show that a minimum core density of roughly 10^5 cm^{-3} is needed to get sufficient shielding from the UV radiation for substantial H₂ formation in the knot. Gould & Salpeter (1963) have shown that H₂ formation is dominated by grain surface reactions for conditions similar to the knots. The Cloudy models confirm this. The grain surface reaction rate used in Cloudy is taken from Cazaux & Tielens (2002b,a). The grain surface formation rate scales linearly with the integrated projected grain surface area. The latter depends critically on the assumed grain size distribution as well as the shape of the grains and the grain abundance. The integrated grain surface area in our models is $\Sigma = 9.78 \times 10^{-22} \text{ cm}^2/\text{H}$. Using other size distributions found in the literature (e.g. Weingartner & Draine 2001) yielded values for Σ with a range of a factor of 5, with our adopted value being towards the upper end of that range. If we assume that the grains have a fractal shape rather than spherical, the projected grain surface area will be larger than assumed above, yielding shorter formation timescales.

The formation timescales from the Cloudy models can be summarized in the fitting formula given in Eq. 1

$$t_{\text{H}_2} = \frac{1170}{n_6^{0.9} \Sigma_{-21}} \text{ [yr]}. \quad (1)$$

Here n_6 is the hydrogen density in the knot in units of 10^6 cm^{-3} and Σ_{-21} is the projected grain surface area in units of $10^{-21} \text{ cm}^2/\text{H}$. O'Dell et al. (2007) state that the central star has exhausted hydrogen-shell nuclear burning one to two thousand years ago. Given the observed core densities in the knots, significant H₂ formation would be possible (though conversion from H⁰ to H₂ need not be complete) assuming that the knot formation was quick after the recombination started and keeping the

uncertainties stated above in mind. Hence this is currently the most plausible explanation for the presence of H₂ in the knots.

Acknowledgements. We thank William J. Henney and Robin J.R. Williams for fruitful discussions. PvH, GVdS, KE, MG, JB, WDM, RH, CJ, SR, PR, and BV acknowledge support from the Belgian Federal Science Policy Office via the PRODEX Programme of ESA. PACS has been developed by a consortium of institutes led by MPE (Germany) and including UVIE (Austria); KU Leuven, CSL, IMEC (Belgium); CEA, LAM (France); MPIA (Germany); INAF/IFSI/OAA/OAP/OAT, LENS, SISSA (Italy); IAC (Spain). This development has been supported by the funding agencies BMVIT (Austria), ESA-PRODEX (Belgium), CEA/CNES (France), DLR (Germany), ASI/INAF (Italy), and CICYT/MCYT (Spain). SPIRE has been developed by a consortium of institutes led by Cardiff Univ. (UK) and including Univ. Lethbridge (Canada); NAOC (China); CEA, LAM (France); IFSI, Univ. Padua (Italy); IAC (Spain); Stockholm Observatory (Sweden); Imperial College London, RAL, UCL-MSSL, UKATC, Univ. Sussex (UK); Caltech, JPL, NHSC, Univ. Colorado (USA). This development has been supported by national funding agencies: CSA (Canada); NAOC (China); CEA, CNES, CNRS (France); ASI (Italy); MCINN (Spain); SNSB (Sweden); STFC (UK); and NASA (USA). Data presented in this paper were analysed using “HIPE”, a joint development by the Herschel Science Ground Segment Consortium, consisting of ESA, the NASA Herschel Science Center, and the HIFI, PACS and SPIRE consortia. This research made use of tools provided by Astrometry.net.

References

- Abel, N. P., Ferland, G. J., Shaw, G., & van Hoof, P. A. M. 2005, *ApJS*, 161, 65
 Aleman, I. & Gruenwald, R. 2004, *ApJ*, 607, 865
 Beckwith, S., Gatley, I., & Persson, S. E. 1978, *ApJ*, 219, L33
 Cazaux, S. & Tielens, A. G. G. M. 2002a, *ApJ*, 577, L127
 Cazaux, S. & Tielens, A. G. G. M. 2002b, *ApJ*, 575, L29
 Ferland, G. J., Korista, K. T., Verner, D. A., et al. 1998, *PASP*, 110, 761
 Ferland, G. J. & Truran, J. W. 1981, *ApJ*, 244, 1022
 Gould, R. J. & Salpeter, E. E. 1963, *ApJ*, 138, 393
 Griffin, M. J., Abergel, A., Ade, P. A. R., et al. 2010, *A&A*, this issue
 Habart, E., Boulanger, F., Verstraete, L., et al. 2003, *A&A*, 397, 623
 Henney, W. J., Williams, R. J. R., Ferland, G. J., Shaw, G., & O'Dell, C. R. 2007, *ApJ*, 671, L137
 Huggins, P. J., Forveille, T., Bachiller, R., et al. 2002, *ApJ*, 573, L55
 Huggins, P. J. & Healy, A. P. 1986, *MNRAS*, 220, 33P
 Lang, D., Hogg, D. W., Mierle, K., Blanton, M., & Roweis, S. 2009, arXiv:0910.2233v1 [astro-ph.IM]
 Liu, Y., Liu, X., Luo, S., & Barlow, M. J. 2004, *MNRAS*, 353, 1231
 Mathis, J. S., Rumpl, W., & Nordsieck, K. H. 1977, *ApJ*, 217, 425
 Matsuura, M., Speck, A. K., McHunu, B. M., et al. 2009, *ApJ*, 700, 1067
 Meaburn, J., Clayton, C. A., Bryce, M., et al. 1998, *MNRAS*, 294, 201
 Meixner, M., McCullough, P., Hartman, J., Son, M., & Speck, A. 2005, *AJ*, 130, 1784
 O'Dell, C. R., Balick, B., Hajian, A. R., Henney, W. J., & Burkert, A. 2003, *Rev. Mexicana Astron. Astrofis. Conf. Series*, 15, 29
 O'Dell, C. R., Henney, W. J., & Sabbadin, F. 2009, *AJ*, 137, 3815
 O'Dell, C. R., Sabbadin, F., & Henney, W. J. 2007, *AJ*, 134, 1679
 Ott, S. 2010, in *Astronomical Data Analysis Software and Systems XIX*, ed. Y. Mizumoto, K.-I. Morita, & M. Ohishi, *ASP Conf. Series*, in press
 Pilbratt, G. L., Riedinger, J. R., Passvogel, T., et al. 2010, *A&A*, this issue
 Poglitsch, A., Waelkens, C., Geis, N., et al. 2010, *A&A*, this issue
 Rauch, T. 2003, *A&A*, 403, 709
 Shaw, G., Ferland, G. J., Abel, N. P., Stancil, P. C., & van Hoof, P. A. M. 2005, *ApJ*, 624, 794
 Speck, A. K., Meixner, M., Jacoby, G. H., & Knezek, P. M. 2003, *PASP*, 115, 170
 Swinyard, B. M., Ade, P. A. R., Baluteau, J.-P., et al. 2010, *A&A*, this issue
 Ueta, T. 2006, *ApJ*, 650, 228
 van Hoof, P. A. M. & Van de Steene, G. C. 1999, *MNRAS*, 308, 623
 van Hoof, P. A. M., Weingartner, J. C., Martin, P. G., Volk, K., & Ferland, G. J. 2004, *MNRAS*, 350, 1330
 Vollmer, B., Gassmann, B., Derriere, S., et al. 2009, arXiv:0912.4174v1 [astro-ph.CO]
 Weingartner, J. C. & Draine, B. T. 2001, *ApJ*, 548, 296

¹ Royal Observatory of Belgium, Ringlaan 3, B-1180 Brussels, Belgium

² Dept of Physics & Astronomy, University College London, Gower St, London WC1E 6BT, UK

³ Instituut voor Sterrenkunde, Katholieke Universiteit Leuven, Celestijnenlaan 200 D, B-3001 Leuven, Belgium

⁴ UK Astronomy Technology Centre, Royal Observatory Edinburgh, Blackford Hill, Edinburgh EH9 3HJ, UK

⁵ Dept. of Physics and Astronomy, University of Denver, Mail Stop 6900, Denver, CO 80208, USA

⁶ Radio Astronomy Laboratory, University of California at Berkeley, CA 94720, USA

⁷ University of Kentucky, Dept. of Physics and Astronomy, 177 CP Building, Lexington, KY 40506-0055, USA

⁸ School of Physics and Astronomy, Cardiff University, 5 The Parade, Cardiff, Wales CF24 3YB, UK

⁹ Space Science and Technology Department, Rutherford Appleton Laboratory, Oxfordshire, OX11 0QX, UK

¹⁰ Dept. of Astronomy, Stockholm University, AlbaNova University Center, Roslagstullsbacken 21, 10691 Stockholm, Sweden

¹¹ Department of Physics, University of Lethbridge, Lethbridge, Alberta, T1J 1B1, Canada

¹² Astronomical Observatory, Valencia University, Edifici Instituts d'Investigació, Parc Científic, C/ Catedrático Agustín Escardino 7, 46980 Paterna (Valencia), Spain

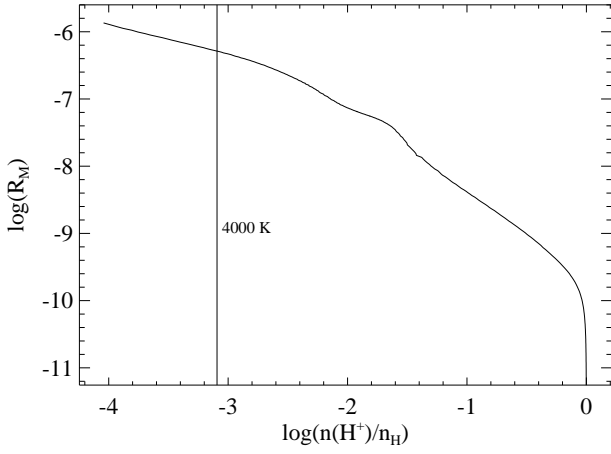


Fig. 2. The H₂ mass fraction as a function of the stopping criterion. The vertical line indicates where T_e reaches 4000 K.

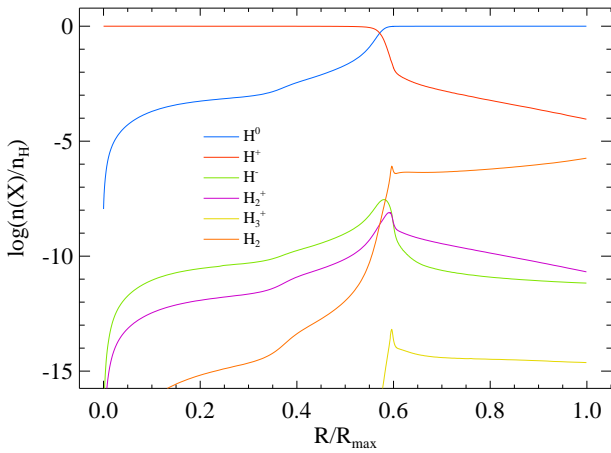


Fig. 3. The standard model of AG04 recreated with Cloudy.

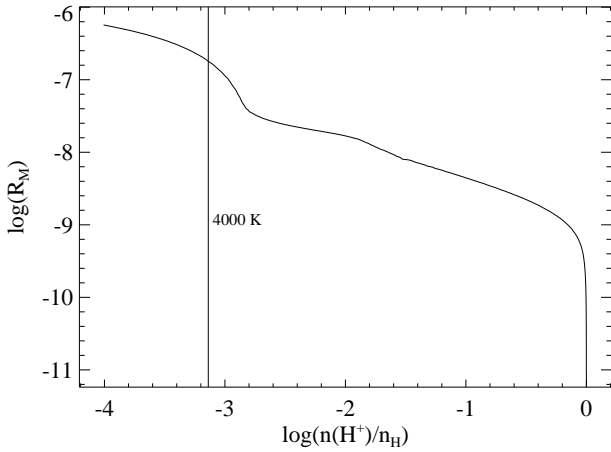


Fig. 4. Same as Fig. 2, but for the standard4 model.

Appendix A: Data reduction

NGC 6720 was observed by PACS in scan map mode (one scan and one cross scan), obtaining maps in the blue (70 μ m) and red (160 μ m) bands. The data were processed with the Herschel Interactive data Processing Environment (HIPE, Ott 2010), following the recommended pipeline for these data. This will be explained in detail in later papers, but a few deviations and customizations are noted here. The WCS has an offset of a few arcseconds that was corrected for the comparison of the PACS map to others (using known sources in the field). We used the version 3 flatfield calibration. The signals were converted to Jy using the version

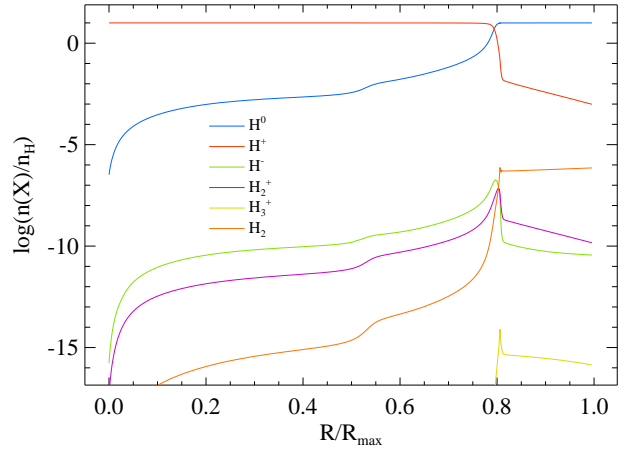


Fig. 5. Same as Fig. 3, but for the standard4 model.

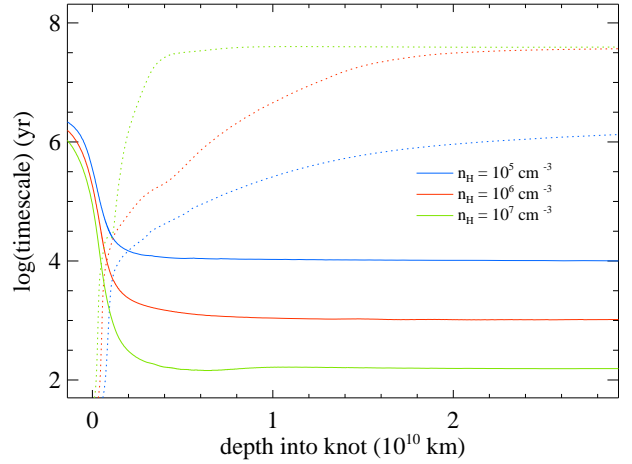


Fig. 6. The H₂ formation and destruction timescales (solid and dotted lines, respectively) for knots with a central density of 10⁵, 10⁶, and 10⁷ cm⁻³ just outside the ionized region.

5 calibration table. We did not remove the cross-talk or corrected for response drifts. Cross-talk correction is not part of the pipeline at present. Response drifts are unlikely to be a problem for our observations: we find no drift in the calibration source signals of more than 1.5% over the duration of the observations. Removal of the glitches (cosmic rays) was done in two stages: first from the regions around our source by filtering along the time-dimension, and then from the source itself working this time on the image plane. Cleaning the maps of the 1/f noise (the name refers to the type of power spectral density the noise has) was done using a high-pass filter method. Here a filter passes over the data as a function of time, subtracting the median of the data over a specified time span (filter width). This allows the high noise frequencies to pass and attenuates the lower frequencies. Considering that moving forward in time means moving along a spatial direction as the instrument is scanning over the source, it is clear that setting a low value for the filter width will rapidly remove varying noise but can have the consequence of removing extended emission. We processed the data with a variety of filter widths, but for our source it made little difference to the photometry or morphology. Also worth noting is that the high-pass filter creates artificial negative "sidelobes" around strong sources. To deal with this the source was masked out before running the high-pass filter. Finally the scan and cross scan frames were combined and turned into a map.

Prior to making the maps presented in this paper the background sources were removed with the HIPE sourceExtractorDaophot task. Slight WCS offsets for the PACS and SPIRE maps were corrected, using background source coordinates measured in the Calar Alto image. The pixel sizes and beam widths are given in Table B.1.

We custom-processed the raw Spitzer data obtained from the archive using both the GeRT and Mosaicker software to remove some obvious anomalies apparent in the pipeline-processed images by following the procedure explained by Ueta (2006).

Table B.1. Aperture photometry of NGC 6720 in various photometric bands. The apertures are elliptical and the semimajor axis is listed in the second column. The fluxes are listed with their measurement and calibration uncertainties, respectively. For the Spitzer data no measurement uncertainties were obtained. The AKARI data were taken from Izumiura et al. (in prep.). The pixel and beam sizes in the Herschel and Spitzer maps are also given.

λ μm	aperture "	flux Jy	pixel size "	beam size "	source
12		0.82 ± 0.07			IRAS
25		10.1 ± 0.5			IRAS
60		$52. \pm 6.$			IRAS
65		$55. \pm 5.$			AKARI
70	150	$59. \pm 7. \pm 6.$	1	~ 5.2	PACS
90		$70. \pm 7.$			AKARI
100		$55. \pm 5.$			IRAS
140		$37. \pm 4.$			AKARI
160	150	$30. \pm 3. \pm 6.$	2	~ 12	PACS
160	152	$28. \pm 7.$	8	~ 40	Spitzer
160		$37. \pm 14.$			AKARI
250	168	$13. \pm 6. \pm 4.$	6	18.1	SPIRE
350	150	$8. \pm 4. \pm 2.$	10	25.2	SPIRE
500	154	$2.2 \pm 1.5 \pm 0.7$	14	36.6	SPIRE

rejected the SWS spectrum as it turned out that the aperture was mainly pointed at the central ‘‘cavity’’ and was therefore strongly biased towards the high excitation region of the nebula. This made aperture correction factors highly dependent on the ionization stage and hence very uncertain. We did use a re-reduced version of the LWS spectrum of NGC 6720, adopting the aperture correction factor listed in Liu et al. (2004). The [O I] lines were excluded from the modeling because they were fitted very badly. A plausible explanation is that these lines are predominantly formed in the knots. We added two dust continuum flux measurements from the LWS spectrum at 43 and 115 μm of 4×10^{-18} and $5 \times 10^{-19} \text{ W cm}^{-2} \mu\text{m}^{-1}$ respectively (aperture correction factors have not yet been applied to these values). We also used two radio continuum flux densities at 4850 and 1400 MHz of 360 and 440 mJy respectively, which are averages of the data collected by Vollmer et al. (2009). For the angular diameter we used 76'' (Liu et al. 2004). We adopted a distance of 740 pc (O’Dell et al. 2009). The model was stopped when the electron temperature dropped below 4000 K. The resulting optimized model has the parameters listed in Table 1. Most symbols have their usual meaning. Γ denotes the dust-to-gas mass ratio and ϵ the logarithmic abundance of an element ($\epsilon(\text{H}) \equiv 12.00$). The electron temperature and density are averaged over the ionized nebula. We will refer to this model as the standard Cloudy model of NGC 6720.

We did the observations of NGC 6720 in the H₂ band by alternating object and sky exposures. We reduced the data in the PixInsight Core package using the acquired bias, dark, flatfield and sky frames. Special care was taken to avoid artifacts in the object frames caused by the presence of stars in the sky frames. A percentile clipping integration was done on the sky frames, grouping them in groups of 5 images. By fitting the average signal of the (already bias, dark and flatfield corrected) sky frames, a tight rejection of outliers was possible, allowing the removal of the stars in the images. Then the resulting sky frame was subtracted from the object frame acquired in the middle of the five sky frames. We corrected the residual background gradients due to sky variation by subtracting a sky background model built with the DynamicBackgroundExtraction module of PixInsight. Finally this image was astrometrically calibrated using the astrometry.net package (Lang et al. 2009).

Appendix B: Photometry

To measure the fluxes from the PACS, SPIRE and Spitzer maps we used an elliptical aperture around NGC 6720. The measured values are given in Table B.1. The PACS data were already in Jy/pix, the SPIRE data were converted from Jy/beam to Jy/pix using the conversion $\pi(\text{beam}/\text{pixel})^2/(4 \ln 2)$ where the pixel and beam sizes are listed in Table B.1. The measured fluxes were also multiplied by factors provided by the SPIRE team as the calibration tables did not yet include these². The Spitzer data were in MJy/sr and were converted to Jy/pix via the conversion given in the MIPS instrument handbook (Sect. 4.3). No additional corrections were applied (e.g. color corrections). Uncertainties are quoted in Table B.1. Calibration uncertainties were taken from the respective instrument guides or release notes. Measurement errors are difficult to calculate, as for these (bolometer) instruments the Poissonian errors are not easily obtained. We combined the contribution of the sky noise, the values in the error arrays which the PACS and SPIRE pipelines create, and the variation in map fluxes that different reasonable pipeline parameter variations gave. For the Spitzer fluxes no measurement uncertainties were calculated.

As the beam size and the pixel scales on the maps are all different we measured all the flux that could be seen from the source down to the sky level, independently for each map. The aperture sizes used are included in Table B.1.

Appendix C: The photoionization model

We used the method described in van Hoof & Van de Steene (1999) to create an optimized photoionization model of NGC 6720 using a prerelease of version C10.00 of the photoionization code Cloudy (revision 3862). The method was slightly modified in that we used H-Ni model atmospheres from Rauch (2003). As input we used the UV and optical spectrum listed in Liu et al. (2004). We

² The SPIRE flux calibration multipliers are: 250 μm : 1.02, 350 μm : 1.05, 500 μm : 0.94.